Available online www.jocpr.com

Journal of Chemical and Pharmaceutical Research, 2017, 9(5):188-200

Research Article

ISSN : 0975-7384
CODEN(USA) : JCPRC5

9-Phenyl Acridine: A Possible Poly (ADP-ribose) Polymerase-1 Inhibitor

Sayantani Karmakar, Debashri Manna, Semanti Ghosh, Surajit Hansda, Anindita Mitra, Angshuman Bagchi and Rita Ghosh*

Department of Biochemistry and Biophysics, University of Kalyani, Kalyani, Nadia-, West Bengal, India

---

ABSTRACT

Poly (ADP-ribose) polymerase-1 (PARP1) is involved in DNA repair, its inhibition can potentiate cell killing by different agents. When used in conjunction, inhibitors of PARP1 can sensitize the action of chemotherapeutic agents thus making PARP1 an attractive target for therapeutic intervention in cancer. Docking of 9-phenyl acridine (ACPH) with human PARP1 (hPARP1) revealed that ACPH could bind by interacting with the catalytically important amino acids at its NAD^+ binding pocket. Its binding free energy was also determined to compare with that of other known inhibitors. Molecular dynamic simulation also established the binding of ACPH at the NAD^+ binding pocket and also revealed its interaction with the catalytically important residues. These findings indicated that ACPH can be a potent hPARP1 inhibitor. In cultured A375 cells, post treatment with ACPH could sensitize cells to killing in both exponential and quiescent cells. NAD^+ is the substrate for hPARP1 in DNA damaged cells; hence depletion of NAD^+ indicates hPARP1 activity. The NAD^+ content of treated cells were determined biochemically. Post treatment with ACPH prevented NAD^+ depletion in the DNA damaged cells confirming its hPARP1 inhibitory activity. Considering the significance of hPARP1 inhibitors not only in cancer therapeutics but in various pathological conditions, the findings could be noteworthy for new drug development.

Keywords: PARP1inhibitor; ACPH; Molecular docking; Molecular dynamic simulation; NAD^+

INTRODUCTION

Acridines are well known for their role in a wide range of biological functions. They have been used for treatment of different diseases arising from viral, bacterial and protozoal infections [1-3] and are also known to exhibit anticancer activities [4]. Acridines generally bind to DNA and interfere with its metabolism to exert its action in cells. The cytotoxic actions of some derivatives are mediated either through its intercalation or groove binding in DNA [5-7] while some other acridine derivatives act by inducing unusual structural changes in DNA [8]. Apart from its interaction with DNA, the acridine moiety can also act on different vital cellular enzymes like telomerase, topoisomerase, cyclin dependent protein kinase, polymerase etc. to exercise its action [9-12]. Although, acridines are known to interact with varied enzymes to exert their inhibitory action, none were known to act on poly ADP ribose polymerases. We found for the first time from preliminary molecular docking studies that 9- phenyl acridine and its derivatives may bind to chicken poly (ADP-ribose) polymerase-1 [13].

Poly (ADP-ribose) polymerase-1 (PARP1) is a 116 KDa conserved protein that constitutes about 85% of the total PARP activity found in cells [14]. Its involvement in different cellular functions is responsible for its role in the physiology of inflammation, stroke, cardiac activity, diabetes and cancer [15]. Therefore, inhibition of its activity finds importance in the therapeutic management for these patho-physiological conditions [15]. The DNA binding domain of PARP1 is about 46 KDa, which is present at its N-terminal end. This is followed by a 22 KDa long auto-modification domain, where the enzyme can form AD- ribosyl polymers onto itself. The catalytic domain of this enzyme stretches over 56 KDa and is located at the C-terminal end. The active site within the catalytic domain contains the NAD^+ binding site [14].

The pivotal role of PARP1 is in DNA damage-repair; its activity is triggered when the cell senses DNA breaks; so it acts as a nick sensor to initiate the synthesis of long, linear and branched, negatively charged poly (ADP-

ribose) (PAR) chains on different nucleosomal proteins and also onto itself, by utilizing cellular NAD^+ as substrate [14]. The process of ADP ribosylation attracts the nucleosomal proteins from the DNA to facilitate repair activity in the cells [14]. Inhibition of PARP1 activity can potentiate cell killing by different damaging agents [16]. Human PARP1 (hPARP1) inhibitors are therefore, important in cancer therapy as it facilitates cell killing.

We have shown earlier that 9-phenyl acridine (ACPH) has anticancer activity in different human cancer cell lines [17]; we therefore, wanted to study thoroughly the interaction of ACPH with hPARP1 to investigate whether its action in cancer cells could be through inhibition of this enzyme. In this report, we present our findings on the binding of ACPH to hPARP1 through molecular docking and molecular simulation studies. Different ligands that bind to PARP1 can either activate or inhibit its action [16,18]. We have shown that ACPH can potentiate cell killing by DNA damaging agents in both exponential and quiescent phase cells to indicate that ACPH could be a potent hPARP1 inhibitor. PARP1 utilizes NAD^+ as its substrate to produce the PAR chain onto different proteins leading to depletion of NAD^+ in PARP1 activated cells. The depletion of NAD^+ is considered as a signature of PARP1 activity in DNA damaged cells [19]. We have demonstrated that ACPH prevented the depletion of NAD^+ in cells with DNA damage. Taken together, these findings revealed the possible role of ACPH as an inhibitor of PARP1.

EXPERIMENTAL SECTION

Generation of Three Dimensional Structures of Ligands and their Docking with PARP1

The three dimensional coordinates of the amino acid residues of wild type hPARP1 protein were retrieved from Protein Data Bank with PDB ID: 4L6S [20]. The coordinates of ACPH and 6 different established inhibitors of PARP1 (nicotinamide, 3AB, PD128763, 4ANI, NU1025 and ABT-888) were generated and optimized in three dimensional spaces using the program ACD/ChemSketch (http://www.acdlabs.com/download/chemsk.html) and the tool PyMOL 7.2 [21]. The saved structures of the ligands were energy minimized by means of Conjugate Gradient (CG) algorithm using the program DISCOVERY STUDIO 2.5 (2013) with CHARMm force field until the structures reached the final energy derivative of 0.001 kcal/mol. CHARMm is the most widely used force-field. It is suitable for proteins, protein-ligand and protein-DNA complexes [22].

The energy minimized coordinates of the ligands were used to dock with the hPARP1 separately using Autodock 4.2 software [23]. For docking the un-protonated forms of the ligands were used. The un-protonated forms would help to prevent undesirable covalent bond formations between the ligand and the protein. This software uses the Lamarckian Genetic Algorithm (LGA). The grid size was set to 126 (maximum grid size) with the X, Y and Z axis having 0.375 Å grid spacing. Apart from this, the energy minimized structures of the ligands were also subjected to docking with hPARP1 separately, using Patchdock server [24] and the program GOLD [25] in order to get a comprehensive result.

From the Autodock results, the lowest binding energy conformation was selected out of the 10 different outputs and analyzed. The docked complexes that yielded the best Goldscore and Chemscore were selected for the GOLD program. The best docked conformations formed from the different software tools used, were again subjected to energy minimization by CG algorithm implemented in the program DISCOVERY STUDIO 2.5 (2013) with CHARMm force field until the structures reached the ultimate energy derivative of 0.001 kcal/mol. This was done in order to remove atomic bad contacts [22].

Molecular Dynamics Simulation (MD Simulation) Study of Wild Type hPARP1 and hPARP1-ACPH Complex

In order to detect the dynamic behavior of the hPARP1-ACPH complex inside the cellular environment, the wild type hPARP1 and wild type hPARP1-ACPH complex were subjected to molecular dynamics simulations using GROMACS 5.0.5 [26] software package in the HP Z840 workstation. The wild type hPARP1 and hPARP1-ACPH complex were simulated in the same cellular conditions. The systems were placed in a triclinic box maintaining a minimum distance of 10Å from the edges of the triclinic. The extended simple point charge (SPC/E) water model was applied for solvation. The simulation in GROMACS was run with the help of GROMOS 53a6 force field. This force field contains all the parameters of CHARMm force field. The systems were neutralized by adding proper counter ions. The dimensions of the box were selected to prevent self-interactions between the different images of the system under consideration. Next the total solvated systems were energy minimized. All bond lengths were constrained using the LINCS method [27], and long-range electrostatic binding interactions were analyzed with the smooth Particle Mesh Ewald (PME) method [28]. The system was equilibrated using position-restrained (PR) equilibration under normal physiological temperature (310 K) and pressure (1 atm) for 100 ps for the wild type PARP1 as well as the docked complex. Trajectory files so generated after completion of the production runs of 30 ns were analyzed accordingly. Analyses of the results from the molecular dynamics simulation runs were done using GROMACS tools, VMD 1.9.1 and DISCOVERY STUDIO 2.5 (2013) software suite. A secondary structure recognition algorithm (DSSP) and the solvent-

accessible surface area (SASA) of binding site were analyzed by 'gmx do dssp' and 'gmx sasa' tools respectively. The program Excel 2007 was used to plot the 2-D data and the 3-D images were created with DISCOVERY STUDIO 2.5 (2013) or Ligplot 1.4.5.

Molecular Properties of the Ligand

The drug like properties of the ligand ACPH was checked using Calculate Molecular Properties (Lipinski drug filter) Protocol in DISCOVERY STUDIO 2.5 (2013). This program was used to check the pharmacological or biological properties of the ligand to ascertain its ability to act as a drug [29].

Cell Culture

A375 human melanoma cell lines were routinely grown in cell culture quality plastic ware (Tarson, India) in minimal essential medium (MEM) (HiMedia, India) supplemented with 10% fetal bovine serum (HiMedia, India). The cells were incubated at 37°C in a humidified atmosphere in presence of 5% CO_2 for growth and sub-cultured twice a week to keep them in an exponentially growing state.

Cell Viability Assay for Exponentially Growing Cells

Viability assay was done as described earlier [30]. Briefly, the medium was aspirated off from the exponentially growing A375 cells, washed with PBS and then irradiated with different doses of UVC (5, 12, 20 J/m^2) from a germicidal lamp (λ=253.7 nm) with or without subsequent treatment with 2 µM of ACPH or 5 mM of 3 amino benzamide (3AB) for 1 h. The treated cells were washed with PBS, trypsinized and subjected to trypan blue exclusion assay using 0.2% trypan blue. While the dead cells were stained blue, the live cells did not take up the stain. The live and dead cells were counted by hemocytometer to estimate the surviving fraction as described earlier [17]. The results shown are the mean from ± SD from three independent experiments.

Cell Viability Assay for Density Inhibited Cells

A375 cells were grown to confluence and held in density inhibited state for 3 to 4 days by replenishing the cells with fresh growth medium. The cell cycle profile was determined in FACS (BD Calibur) to ascertain that the cells were in density inhibited quiescent condition. The medium was aspirated off and the cells were washed in PBS before harvesting by trypsinization. The cells were then centrifuged at 2500 rpm for 5 mins and the supernatant was discarded. The cell pellet was gently dislodged before fixing in chilled 70% ethanol for 1 h. This suspension was again centrifuged after 1 h at 2500 rpm for 5 mins to remove the alcohol. The cell pellet was again suspended in PBS with 10 µg/ml RNase A (Sigma) and kept in a water bath at 37°C for 30 mins. Next, the cells were stained with 10 µg/ml PI (Sigma) and kept for 15 mins at room temperature in the dark. Finally, the analyses were performed in FACS (BD Calibur) using Cell-Quest Pro software (BD) [31].

Viability assay was done with parallel sets of such cells. The medium was aspirated off and the cells were washed with PBS before exposing them to different doses of UVC (λ=253.7 nm) (12, 20 and 24 J/m^2) without or with subsequent treatment with 2 µM of ACPH or 5 mM of 3AB for 1 h. After the treatments, the cells were rinsed in PBS, trypsinized and the viability of these quiescent cells was assayed both immediately and after 24 h using trypan blue exclusion assay. The results shown are the mean ± SD of three experiments.

Nicotinamide Adenine Dinucleotide (NAD^+) Assay

2-4 $\times 10^5$ exponentially growing A375 cells were exposed to 12 J/m^2 of UVC dose followed by treatment with 2 µM of ACPH or 5mM of 3AB for different time period (0, 30, 60, 120 and 180 mins) before NAD^+ assay [30]. After the treatment, the cells were washed twice with ice cold PBS, acidified with 1 ml of 0.5 M $HClO_4$ and kept on ice for 20 mins. From the acid supernatant, 900 µl was collected, neutralized with 450 µl of 1 M KOH, 0.33 M K_2HPO_4/KH_2PO_4, pH 7.5 and again allowed to stand on ice for 20 mins. The $KClO_4$ was precipitated by centrifugation at 10,000 rpm for 5 mins at 4°C and the supernatant was collected. 350 µl of supernatant was mixed with 310 µl reaction mixture (containing 60 µl Bicine 1.2 M pH 7.8 (HiMedia, India); 60 µl of BSA 10 mg/ml (Sigma, USA); 60 µl EtOH 6M; 6 µl EDTA 500 mM (HiMedia, India); 60 µl phenazineethosulfate 20 mM (Sigma, USA); 60 µl MTT 5 mM (Sigma, USA) and 4 µl H_2O) and incubated at 30°C for 5 mins in the dark. Then, alcohol dehydrogenase (60 µl, 1 unit/ml, Sigma, USA) was added and incubated at 30°C in the dark for 30mins for color development. Next, 300 µl of 12 mM iodoacetate (HiMedia, India) was added, and finally the absorbance was monitored at 570 nm in a spectrophotometer (Shimadzu, UV-1601, India). The experiment was repeated in triplicate.

RESULTS

Binding of ACPH to hPARP1

The binding of ACPH to hPARP1 is shown in Figure 1; a close-up view showing the amino acid residues with which ACPH interacts are shown at the inset.

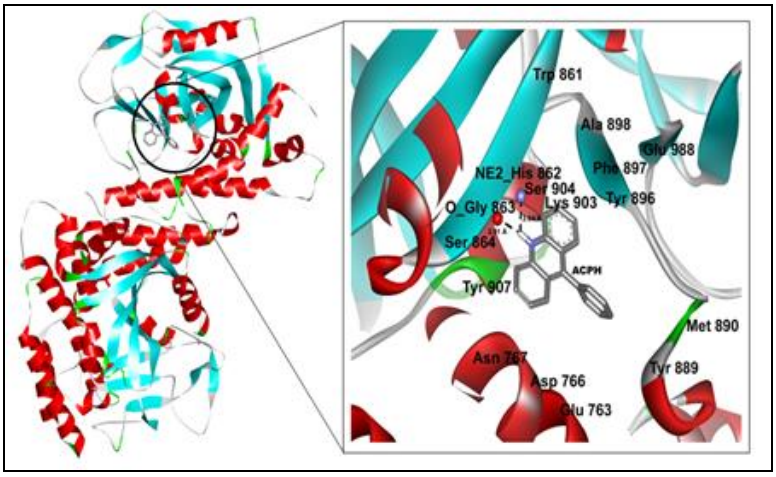

Figure 1: The figure represents the binding of ACPH to PARP1; the close-up view shows the amino acid residues with which ACPH interacts

The different amino acid residues lining the NAD^+ binding pocket of the enzyme, viz. Asp766, Asn767, Trp861, His862, Gly863, Ser864, Met890, Tyr896, Phe897, Ala898, Lys903, Ser904, Tyr907, His909 and Glu988 were found to be lying within a radius of 5Å from this ligand. This would indicate their interactions at the NAD^+ binding site. The ligand, ACPH formed two H-bonds; one with NE2 atom of His862 (3.04Å) and the other with the O atom of Gly863 (2.01Å); it also showed π-π interaction with the aromatic ring of Tyr907. The binding free energy of ACPH was -32.4937 kcal/mol.

A comparison was also made between the binding of ACPH to hPARP1 with that of nicotinamide, 3AB, PD128763, 4ANI, NU1025 and ABT-888 to hPARP1. From the analyses of the binding interactions of the other ligands with hPARP1, it was revealed that ACPH binds at the same location of hPARP1 as these established inhibitors. The interaction of these inhibitors with the different amino acids of hPARP1 is shown in Table 1.

Comparison between the interaction of hPARP1 and ACPH with that for the other inhibitors revealed that the binding free energy of ACPH to hPARP1 was the best (-32.4937 kcal/mol); this is shown in Figure 2.

Table 1: The interaction of ACPH and the other PARP1 inhibitors

Inhibitors	Interacting residues with PARP1 at the NAD^+ binding site
ACPH	Glu763, Asp766, Asn767, Trp861, His862, Gly863, Ser864, Met890, Tyr896, Phe897, Ala898, Lys903, Ser904, Tyr907, His909, Glu988
Nicotinamide	Trp861, His862, Gly863, Ser864, Tyr896, Phe897, Ala898, Lys903, Ser904, Tyr907, Asn987, Glu988, Tyr989
3 Amino-Benzamide	Glu763, Trp861, His862, Gly863, Ser864, Met890, Tyr896, Phe897, Ala898, Lys903, Ser904, Tyr907, Glu988
PD128763	Trp861, His862, Gly863, Ser864, Tyr896, Phe897, Lys903, Ser904, Tyr907, Asn987, Glu988, Tyr989
4ANI	Glu763, Trp861, His862, Gly863, Ser864, Tyr889, Met890, Tyr896, Phe897, Ala898, Lys903, Ser904, Tyr907, Glu988
NU1025	Glu 763, Asp 766, Asn 767, Gly 888, Tyr 889, Met 890, Tyr 896, Lys 903, Tyr 907, Glu 988
ABT-888	Glu 763, Asp 766, Asn 767,Trp 861, His 862, Gly 863, Ser 864,Arg 878, Tyr 889, Tyr 896, Phe 897, Ala 898, Lys 903, Ser 904, Tyr 907, His 909, Glu 988

The amino acid residues that are important for the catalytic activity of PARP1 are mainly His 862, Gly863, Lys903, Ser904, Tyr907 and Glu988. ACPH and all these other inhibitors were found to interact with these residues. When we introduced *in silico* mutations in these amino acid residues, ACPH either could not recognize this pocket (E988K and E988A) or even when it could recognize (K903A, Y896N, Y896A, Y907A, and G863A), its binding affinities were much lower, as revealed from the binding free energies as shown in Table 2 and Figures 3a-3d. These findings indicate that the interactions of ACPH with these catalytically important residues were pivotal for its binding to native PARP1.

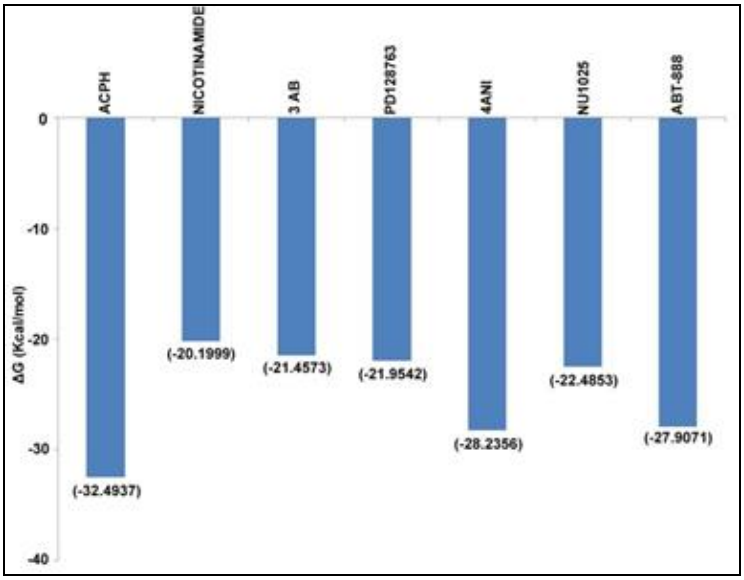

Figure 2: The binding free energy values obtained with the interaction of PARP1 with ACPH and the other inhibitors are represented graphically in the figure

Table 2: The mutations induced to PARP1 protein via *in silico* mutagenesis, the site of ACPH binding to the mutants along with their binding free energies are listed

Mutations	Site of ACPH binding	Figure numbers
E988K	Remote from the catalytic site	Figure 3a
E988A	Remote from the catalytic site	Figure 3b
K903A	At the NAD^+ binding pocket; disfavored binding (BFE= +1.9227 kcal/mol)	Nil
Y896A	At the NAD^+ binding pocket; disfavored binding (BFE= -7.7063 kcal/mol)	Figure 3c
Y907A	At the NAD^+ binding pocket; highly disfavored binding (BFE= +11.9549 kcal/mol)	Nil
G863A	At the NAD^+ binding pocket; weaker binding (BFE= -10.9974 kcal/mol)	Figure 3d

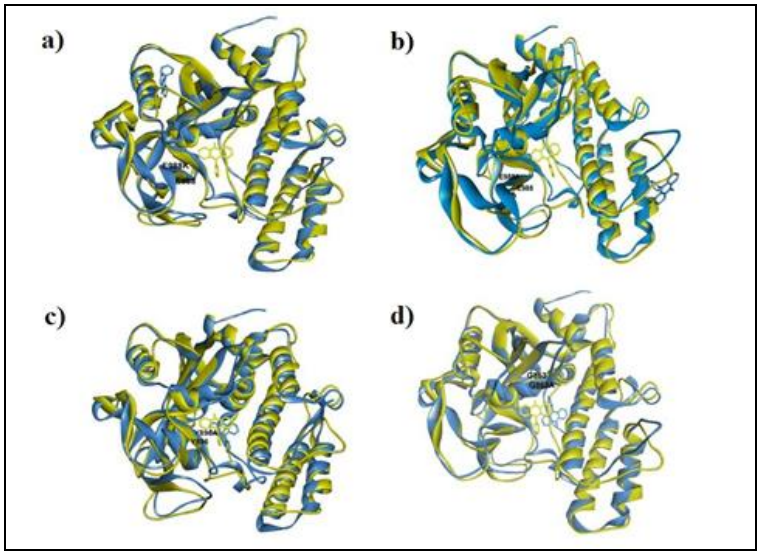

Figure 3: The figure depicts the remote binding of ACPH from the catalytic site of hPARP1 when a) E988K; b) E988A; c) Y896A and d) G863A mutations were inserted. The wild type protein along with the ligand was colored yellow and the mutated protein along with the ligand was colored blue. The protein and the ligand structures were in secondary ribbon form and stick form respectively

Molecular Dynamics Simulation (MD simulation) study of Wild Type hPARP1 and hPARP1-ACPH Complex

Both wild type hPARP1 and hPARP1 bound to ACPH were found to be stabilized after 15 ns of dynamics run for 30 ns. The completions of the dynamics run for both the systems were calculated by the root mean square deviation (RMSDs) of the backbone atoms during the simulation runs. It was shown that initially the hPARP1 protein in the unbound state had lower backbone RMSD (around 3 Å) as compared to the hPARP1 bound to

ACPH (around 6 Å). However, after stabilization, hPARP1-ACPH complex was found to be more stable than the hPARP1 protein itself. This indicated that after ACPH binds to the wild type hPARP1, the complex becomes more stable (maximum backbone RMSD was 4 Å) than unbound state (maximum backbone RMSD 6 Å) (Figure 4a). The hPARP1-ACPH complex shows the radius of gyration stability after 18 ns of simulation run (Figure 4b) which also signifies the stability of protein compactness after ACPH binding. The whole analyses were done from 15 to 30 ns stable region of the dynamics. The PDB coordinates were stripped out from these stable regions and the interaction energies of the amino acids present in the binding interface were studied. When root mean square fluctuation (RMSF) profiles of C-α atoms were analyzed throughout simulation for ACPH bound hPARP1, we observed that amino acid region 670-742, 750-765 (mild changes), 780-785, 790-850 and 865-910 showed fluctuations between bound and unbound hPARP1 protein (Figure 4c). The amino acid residues of these regions were also present at the binding interface of ACPH and showed high interaction energies. Some of the active site residues of hPARP1-ACPH complex actively participated in non-bonded interactions i.e., Van der Waals interactions with the ACPH. The binding interface of the stable-most structure of hPARP1-ACPH complex from MD simulation was found to contain the amino acid residues Val758, Gln759, Ala760, Val762, Glu763, Asp766, Asn767, His862, Gly863, Arg878, Pro885, Gly888, Tyr889, Met890, Tyr896, Lys903, Tyr907, Asn906, His909, Glu988.

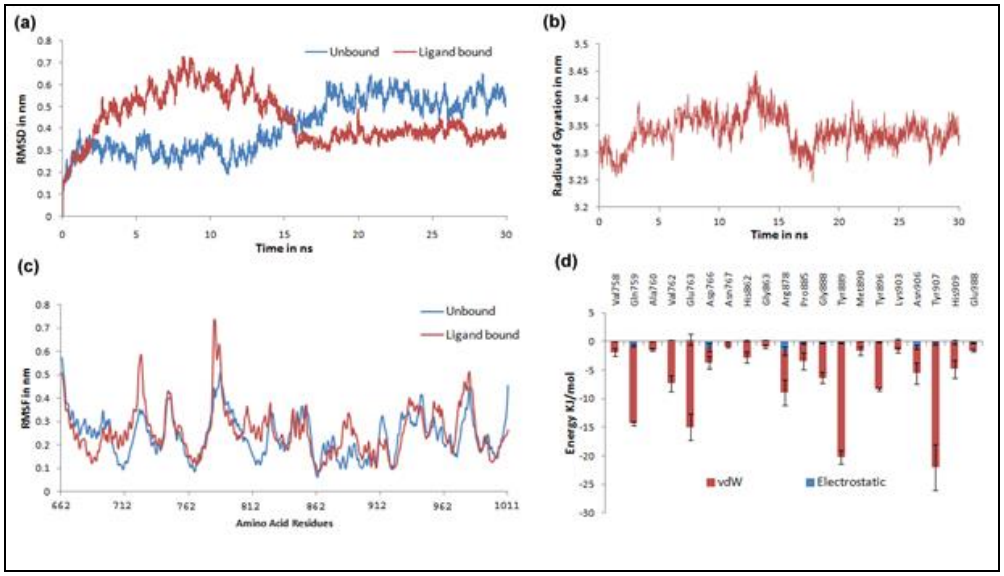

Figure 4: a) Stability differences between unbound PARP1 and ACPH bound PARP1; b) Gyration stability of ACPH bound PARP1 complex; c) Fluctuations in amino acid regions between bound and unbound PARP1; d) Amino acid residues with high total interaction energy making the bound PARP1 more stable

However, the MD studies also revealed that the amino acid residues which were involved in interactions with hPARP1 maximally were Gln759, Val762, Glu763, His862, Glu863, Ser864, Arg878, Gly888, Tyr889, Tyr896, Lys903, Asn906, His909 that showed high interaction energies than other active site residues thereby making the ligand bound complex stable (Figure 4d).

The binding free energy and solvent accessible surface area (SASA) were calculated throughout the course of molecular dynamics simulation. The ligand binding free energy values ranged between -52.58 to -59.0344 kcal/mol throughout the MD simulation (Figure 5a) having an average value of -55.6883 kcal/mol (Figure 5b). These values indicated a stable ligand binding state for this enzyme that was much higher than any other inhibitor molecules of hPARP1. There was a decrease in the solvent accessible surface area between the unbound and ligand bound hPARP1 complex (Figures 5c and 5d) signifying the compactness of the hPARP1 protein after ligand binding, which can now be co-related with stable gyration of this complex.

It was further revealed that the conformations of hPARP1 and hPARP1-ACPH complex were highly dissimilar as observed by the calculations of the backbone RMSD value between the proteins, which was found to be 6.361 Å (Figure 6a). The binding interface residues of the PARP1 protein are shown in Figure 6b. So, MD simulation studies confirmed that the wild type PARP1 actively interacts with ACPH to form a stable complex.

Molecular Properties of the Inhibitors by Lipinski Rule of Five (RO5)

The Lipinski rule of five states the five rules which are important for a molecule to become a drug. Considering these parameters, it was found that ACPH has 1 hydrogen bond donor, 1 hydrogen bond acceptor, molecular mass of 257.32 g/mole and the AlogP value is 4.076. The Lipinski rule for the other 6 established inhibitors were also checked and listed in Table 3 for comparison.

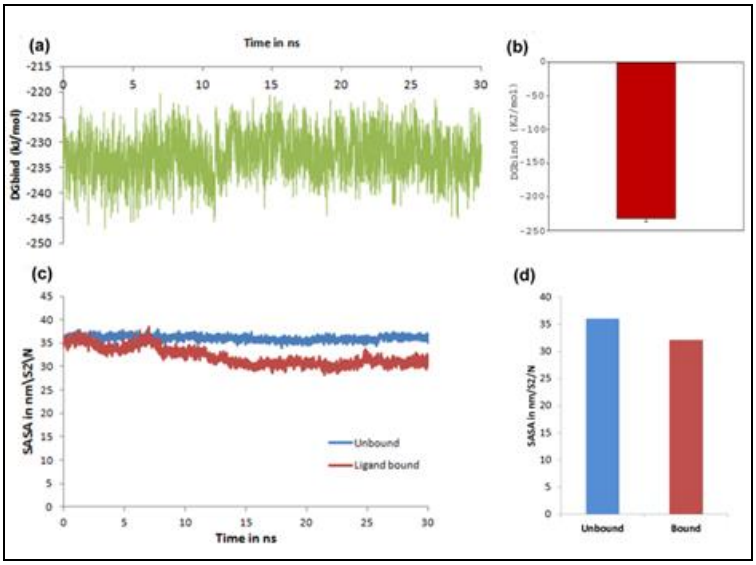

Figure 5: a) Ligand binding free energy throughout simulation; b) stable ligand binding energy; c,d) SASA energy value difference between bound and unbound PARP1 complex

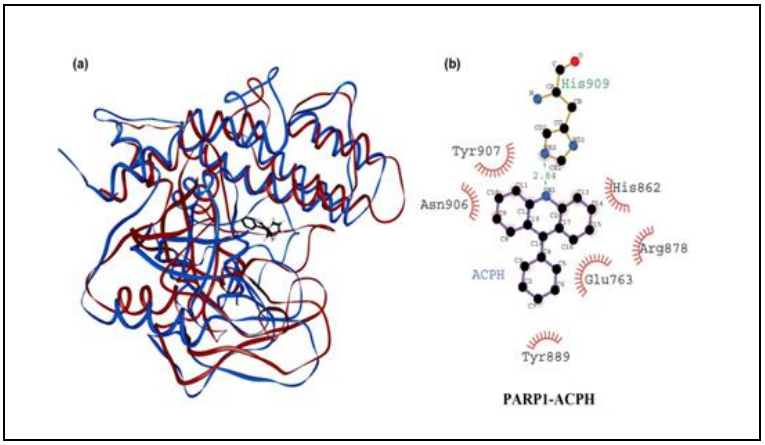

Figure 6: a) The superimpositions of the stable most conformations from simulations of ACPH bound and unbound PARP1 protein; b) the binding interface residues of the ACPH bound stable most conformations from simulation with H-bond

Table 3: The parameters to check whether ACPH can act as an orally active drug through Lipinski Rule in comparison with other PARP1 inhibitors

Molecular properties	Name of the inhibitors						
	ACPH	**Nicotinamide**	**3 Amino Benzamide**	**PD128763**	**4ANI**	**NU1025**	**ABT-888**
ALogP	4.076	-0.319	0.085	1.112	0.818	0.508	-0.244
Molecular Weight	257.329	122.125	136.151	147.174	212.204	162.145	245.3
Number of H-Acceptors	1	2	2	1	3	3	2
Number of H-Donors	1	1	2	1	2	2	3
Number of Rotatable Bonds	1	1	1	0	0	0	2
Number of Rings	4	1	1	2	3	2	3
Number of Aromatic Rings	2	1	2	1	2	1	2

The rule justified that ACPH has the ability to act as an orally active drug for humans.

Effect of ACPH and 3AB on Viability of Exponentially Growing A375 Cells Exposed to UVC

A nontoxic dose of 2 µM for 1 h was used for treatment after UV exposure. Exponentially growing A375 cells were exposed to different doses of UVC followed by treatment with 2 µM ACPH. Figure 7 depicts the comparative effect of 2 µM ACPH and 5 mM 3AB on UV induced cell killing. Exposure to 20 J/m^2 of UVC resulted in a cell survival of 61%. Cell killing was sensitized in presence of both 3AB (5 mM) and ACPH (2 µM), where surviving fraction dropped to 35% and 20% respectively. Thus, it showed that ACPH could effectively sensitize cell killing in exponentially growing cells.

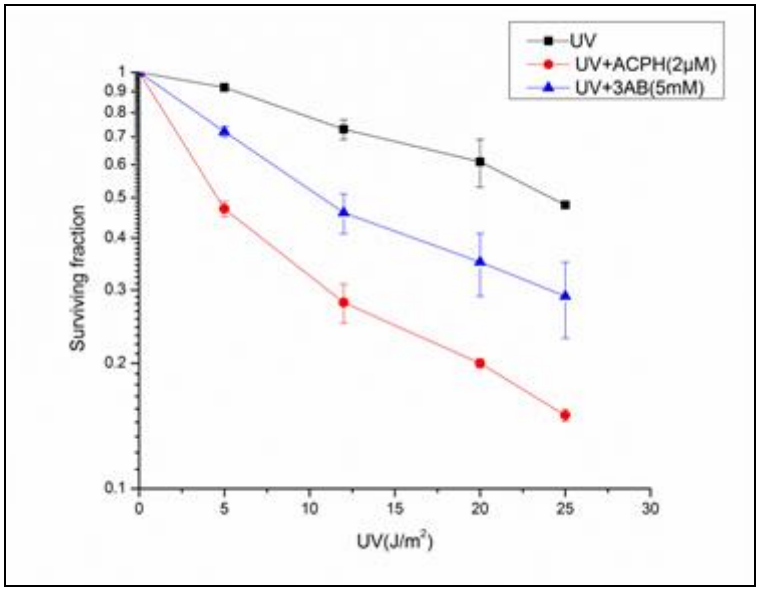

Figure 7: Survival curve of exponentially growing A375 cells. (—■—) represents effect of different doses of UVC (5, 12, 20 J/m^2) on A375 cells, (—●—) represents effect of post treatment of 2 μM ACPH on UV treated cells,(—▲—) represents effect of post treatment of 5 mM 3AB on UV treated cells. Each value represents the mean ± SD (n ≥ 3). Significance levels were calculated according to Student's t-test. *P<0.0001, **P=0.001 and ***P=0.01, compared to UV treated cells

Cell Cycle Distribution of Exponential and Confluent A375 Cells using Flow Cytometry

Figure 8 shows the cell cycle profile of exponential (a) and confluent (b) cell culture. The histogram indicated the percent population of cells at different phases. The absence of the mitotic population in G2/M cells in Figure 8b indicated that the cells were indeed in density inhibited condition.

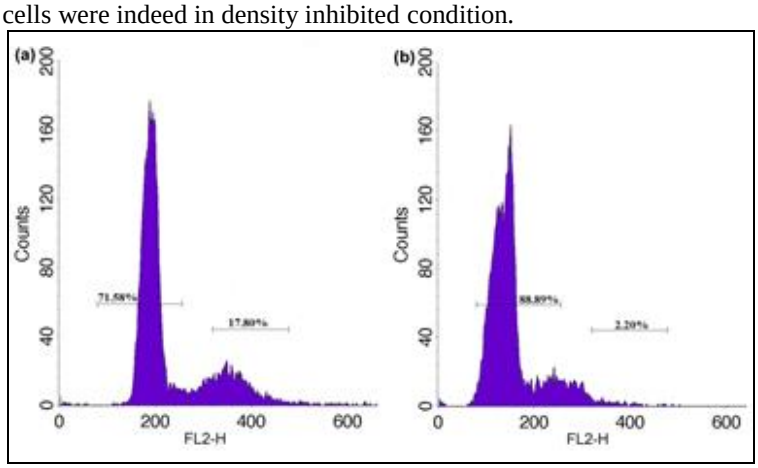

Figure 8: Cell cycle distribution of A375 cells in a) exponential and b) quiscent phases

Effect of ACPH and 3AB on Viability of Quiescent A375 Cells Exposed to UVC

Figure 9 shows the effect of ACPH and 3AB on UVC induced cell killing in confluent, density inhibited A375 cells. Density inhibited cells are proficient in repair through potentially lethal damage repair (PLDR) activity. At a dose of 24 J/m^2 of UVC, the surviving fraction was 62% for these cells; holding the cells in quiescence for a further period of 24 h increased it to 84%, due to more time for PLDR. Both ACPH (2μM) and 3AB (5mM) could sensitize these cells to killing possibly through inhibition of PLDR. For the same dose of UVC, the surviving fraction was 65% and 39% for 3AB and ACPH respectively.

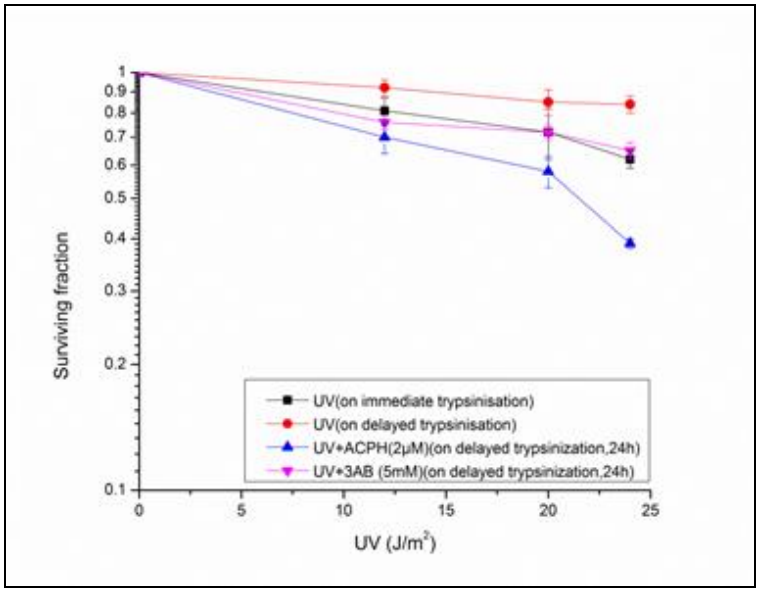

Figure 9: Survival curve of quiscent phase A375 cells. (■) represents effect of different doses of UVC (5, 12, 24 J/m^2) on quiscent phase cells A375 cells on immediate trypsinisation, (●) represents effect of different doses of UVC on delayed trypsinisation, 24 h, (▲) represents effect of post treatment of 2 µM ACPH on UV treated cells after delayed trypsinisation, 24 h, (▼) represents effect of post treatment of 5 mM 3AB on UV treated cells after delayed trypsinisation, 24 h. Each value represents the mean ± SD (n≥ 3). Significance levels were calculated according to Student's t-test. *P= 0.0002, compared to UV treated cells

Effect of ACPH and 3AB on the Intracellular NAD$^+$ Level of Exponentially Growing A375 Cells Exposed to UVC

Figure 10 shows the effect of ACPH on the intracellular NAD$^+$ activity in UVC (12 J/m^2) exposed A375 cells. Exposure of these cells to UVC resulted in depletion of the intracellular NAD$^+$ in a time dependent manner. The presence of 2 µM ACPH or 5mM 3AB could prevent this depletion in NAD$^+$ content in the cells.

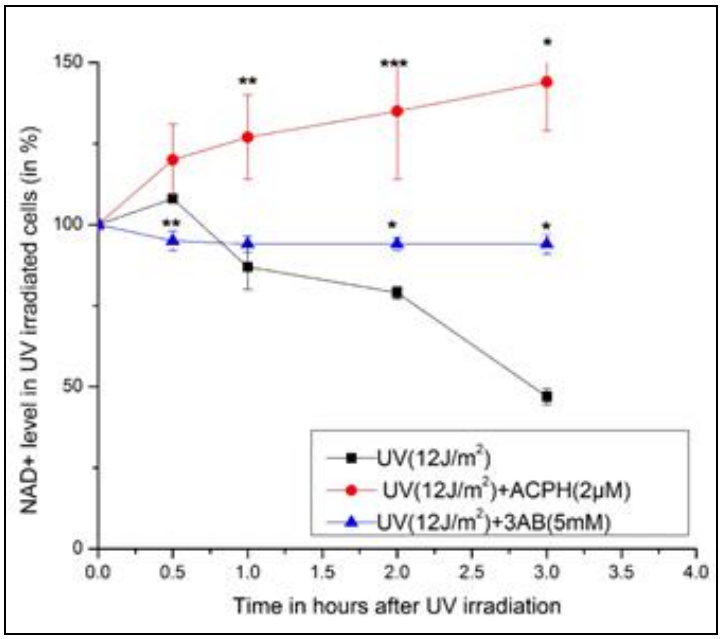

Figure 10: Temporal assay of NAD$^+$ level in exponentially growing A375 cells. (■) represents UVC treatment (12 J/m^2) in A375 cells, (●) represents post treatment of 2 µM ACPH on UV treated cells, (▲) represents post treatment of 5 mM 3AB on UV treated cells. Each value represents the mean ± SD (n ≥ 3). Significance levels were calculated according to Student's t-test. *P<0.0001, **P<0.001 and ***P<0.01, compared to UV treated cells

DISCUSSION

Preliminary docking studies had indicated earlier that ACPH may binds to PARP1 from chicken [13]. Human PARP1 has nearly 87% sequence identity with chicken PARP1. Thus, the overall structures of human and chicken PARP1 would be quite similar. Yet, the remaining dissimilarity between the proteins might lead to

some differences as observed in case of some other proteins in PDB [31]. Thus we tried to analyze the three dimensional structure of PARP1 from human to analyze its mode interactions with the ligand. Our findings revealed that ACPH could also bind to hPARP1 at the NAD^+ binding pocket in its catalytic domain. The binding free energies of PARP1 docked with ACPH and other 6 established inhibitors like nicotinamide, 3AB, PD128763, 4ANI, NU1025 and ABT-888 were also calculated. Compared to the other known inhibitors of PARP1, ACPH showed the best binding free energy value of -32.4937 kcal/mole. The binding free energy values for the other inhibitors ranged between -20 to -28 kcal/mol (Figure 2). The total interaction energies of all docked complexes were also calculated. It was found that the interaction of ACPH (-27.44344 kcal/mol) was comparable with that of other inhibitors complexed with hPARP1. When both hPARP1 and hPARP1-ACPH docked complexes were subjected to molecular dynamics simulation, a comparison of the backbone RMSD values showed that ACPH bound complex was much more stable having an average binding free energy of -55.6883 kcal/mole (-233 kJ/mol). The molecular dynamics simulations would mimic the changes that might occur within a cellular system whereas the docking of protein with ligand would involve a snapshot of the binding interactions. Therefore, MD simulations would come up with a better binding interaction resulting in the stability of the docked complex which was justified by simulating the entire system in an environment mimicking the cellular systems [32]. This binding free energy of ACPH calculated from MD simulations was found to be better than that for Olaparib (-159.16 kJ/mol), a FDA approved inhibitor of PARP1 or ZINC67913374 (-177.28 kJ/mol), a natural product that has been identified by Li et al. through *in silico* screening as a novel PARP1 inhibitor [33]. The binding free energy value of ACPH with hPARP1 was found to be high as observed in other hPARP1-ligand complexes [33,34]. Thus, from determination of binding free energy of the docked complex of hPARP1 and ACPH, it appeared that ACPH can be an effective inhibitor for hPARP1. From MD simulation studies, the stable gyration of the complex and lower solvent accessible surface area depicted a better compactness of the protein folding and proper binding of ACPH. The amino acid residues of hPARP1 protein that are actively involved in ligand binding were Gln759, Val762, Glu763, Asp766, His862, Arg878, Pro885, Gly888, Tyr889, Tyr896, Asn906, Tyr907 and His909 that showed high interaction energies. It was also revealed that the aforementioned amino acid residues had comparatively low RMSF during the entire simulation run (Figure 4d). The low values of RMSF would indicate that the amino acids would remain bound to the ligand during the simulation run [35]. So, from the molecular dynamics study of hPARP1-ACPH bound complex, it could be safely concluded that hPARP1 has complete binding affinity towards ACPH and generated a stable conformation after simulation.

At the C-terminal end of the hPARP1 enzyme, the active site spans over the amino acids 655-1014. Within this site, the location where NAD^+ binds and donates the ADP- ribose moiety is known as the NAD^+ binding pocket or the donor site and the position where the ADP-ribose moieties join to form the PAR chain is known as the acceptor site [36]. The active site is lined by the residues Tyr710, Gln763, Asp766, Asn767, Asp770, Trp861, His862, Gly863, Ser864, Arg878, Ile879, Ala880, Gly888, Tyr889, Met890, Gly894, Tyr896, Phe897, Ala898, Lys903, Ser904, Tyr907, His909, Asn987, Glu988, Tyr989 [37]. Amongst these residues, Gly863, Tyr907 and Glu988 are important among the conserved amino acid residues within species that are important for the enzyme's catalytic activity [38], while some non-conserved amino acids of hPARP1 like, Lys903 and Ser904 are also important for the catalytic activity [39]. ACPH interacted with the amino acid residues Gln763, Asp766, Asn767, Trp861, His862, Gly863, Ser864, Met890, Tyr896, Phe897, Ala898, Lys903, Ser904, Tyr907, His909 and Glu988, all of which are known to be present at the ligand binding interface of hPARP1 i.e., at the NAD^+ pocket. All the established inhibitors of PARP1 and ABT-888 are also known to interact with these amino acids [40]. PARP1 inhibitors like nicotinamide, 3AB, PD128763, 4ANI, NU1025 and ABT-888 are known to interact with Gly863 through H-bonds [40]. Mutating Gly863 to G863A resulted in a weaker binding of ACPH thus indicating that the H-bonding with Gly863 is necessary for binding of ACPH to hPARP1. ACPH also formed H-bonds with O-atom of Gly863 and NE2 atom of the adjacent His862 [40].

Tyr907 lies on the wall of the NAD^+ binding pocket [40]. It is one of the critical amino acid necessary for the catalytic activity of the enzyme. It has been shown that mutating Tyr907 to asparagine resulted in 99% reduction in its activity [41]. It has been predicted that the interactions of ligands with Tyr907 and Gly863 are the key features for the inhibitory action of a number of inhibitors. Novel PARP1 inhibitors like benzo [b] [1,4] oxazin-3(4H)-ones, tricyclic quinoxalinone, cyclic derivatives of benzamide undergoes π-π interaction with Tyr907 [20,42]. ACPH also participated in π-π interaction with the aromatic ring of Tyr907. Furthermore, from the MD simulation of the hPARP1-ACPH complex it was revealed that Tyr907 had the maximum binding interaction energy with the ligand throughout the entire MD simulation. When Tyr907 was converted to asparagine through *in silico* mutation it showed a disfavored binding of ACPH. So it can be concluded that π-π stacking interaction is critical for the binding of ACPH to hPARP1.

A glutamic acid residue is believed to be important for poly ADP ribosylating activity, as a glutamic acid is not only found to be conserved in PARP1 from across all the species, but it is also found in several bacterial toxins like pertussis toxin, DT toxin, cholera toxin and toxin from *Clostridium limosum*, which also perform the same function of joining ADP-ribose units [43]. In hPARP1, it is the Glu988 residue that is responsible for this

function. Mutations in this residue severely reduced the ADP-ribosylating activity of the enzyme [43]. It has been shown that mutation at Glu988 reduced the enzyme's activity to 0.2% of that of the wild type [41]. Our results showed that when Glu988 is replaced *in silico* with either alanine or tyrosine, ACPH could bind weakly at a site that was distant from the NAD^+ binding pocket. This indicated that interaction with Glu988 was essential for appropriate binding of ACPH.

Lys903 and Ser904 were the other catalytically important amino acids. Mutation of K903A resulted in almost complete loss of activity [41]. It was observed that binding of ligands to Lys903 and Ser904 at the NAD^+ binding pocket were important in the inhibitory interaction of 4ANI, PD128763, NU1025 and tricyclic PARP1 inhibitors [44]. 4ANI prevents binding of NAD^+ to PARP1 by forming H-bond with Ser 904 [40]. PD128763 forms H-bond with Lys903 to strengthen its binding specificity [40]. ACPH interacted with both Lys903 and Ser904. K903A mutation resulted in disfavored binding of ACPH at the catalytic site. Thus, although ACPH does not form H-bond with Lys903 and Ser904, its interaction with these amino acids was significant and crucial for its binding to hPARP1.

Another amino acid responsible for creating the hydrophobic pocket at the catalytic site of PARP1 is Tyr896. Y896N mutation significantly dropped the enzyme's activity to 15% [41]. Benzamidazoles, tricyclic lactam indoles, AG14361, olaparib, ZINC67913374 interacted with Tyr896 to exert their inhibitory action [44], ACPH too was found to interact with Tyr896 at the NAD^+ binding pocket. Results from *in silico* mutation analysis revealed that Y896N mutation led to a disfavored binding of ACPH at the NAD^+ binding pocket. Therefore, we can clearly say that Tyr896 is necessary for effective participation of ACPH at the NAD^+ binding pocket.

The findings indicated that ACPH binds at the NAD^+ site of hPARP1 to interact with all the catalytically important amino acids like all other known inhibitors. ACPH therefore has the potential to act as a hPARP1 inhibitor by competing with NAD^+ for binding at the active site.

PARP1 is essential during initiation of different DNA repair pathways; therefore, inhibition of this enzyme with small molecules can induce lethality in DNA damaged cells by preventing repair [45]. We had used UVC as the DNA damaging agent. Post treatment of cells with 2 µM ACPH after UVC irradiation resulted in potentiating of cell killing. UVC alone has an IC_{50} value of 22 J/m^2; in presence ACPH this was lowered to 4 J/m^2. 3AB was also used for comparison and it was found that in presence of 3AB (5 mM) the IC_{50} value was only 10 J/m^2. Thus, ACPH was highly effective in sensitizing cell killing through its PARP1 inhibitory activity at a much lower concentration.

The repair activity in damaged cells can be manipulated by modifying the post irradiation environment condition. If cells are prevented from dividing for an extended period of time after DNA damage, then the cells can survive better through the process of potential lethal damage repair (PLDR). Hence, quiescent cells exhibit greater survival in comparison to exponentially dividing cells [46]. Quiescent cells are model for cells in solid tumors as they are more resistant to killing [47]. PARP1 is also involved in PLDR [46]. 3AB, PD128763, NU1025 and AG14361 have been shown to sensitize cell killing through inhibition of PARP1 to prevent PLDR [44]. ACPH was also found to potentiate cell killing in quiescent A375 cells. The results indicated the efficacy of 2 µM ACPH in potentiating cell killing was better than that of 5 mM of 3AB. These findings are significant as it indicated that ACPH can be effective in inducing cell death even in solid tumors through PARP1 inhibition.

Involvement of PARP1 in DNA repair as well as in regulation of transcription is now recognized to be important for cell survival and death. From different *in vitro* and *in vivo* findings, it has been suggested that PARP1 inhibitors can be used as a single agent to kill cancer cells [48]. The IC_{50} value for different PARP1 inhibitors alone in various cell lines has been determined. For most inhibitors like 3AB, benzamide, NU1025, PD128763, the IC_{50} values are in the milimolar range (6.7 mM, 2.5 mM, 0.41 mM, 0.45 mM respectively) [48]. The IC_{50} values have been determined for AG14361, ABT-888 and olaparibin different pancreatic cancer cell lines and was found to be much lower than the previous inhibitors mentioned; for AG14361, it was 14.3 µM, 12.7 µM, 38.3 µM, with ABT-888, it was 52.6 µM, 100.9 µM, 102 µM and for olaparib, it was 79.5 µM, 184.8 µM, 200.2 µM in CFPAC-1, BXPC-3 and HPAC cell lines respectively [49]. Our laboratory has reported earlier that ACPH has IC_{50} values of 18.5 µM and 20.74 µM in HeLa and A375 cell lines respectively [17]. This indicated the efficacy of ACPH.

The findings from the temporal assay of cellular NAD^+ confirmed the inhibitory role of ACPH against PARP1. PARP1 utilizes NAD^+ as a substrate to form the PAR chain on different proteins, resulting in depletion of intracellular NAD^+ level. Thus depletion of NAD^+ content in cells is widely used to assess the PARP1 activity of cells [44]. Upon DNA damage, PARP1 activity is triggered and therefore there is reduction of NAD^+ in damaged cells [44]. In exponentially growing A375 cells, exposure to UVC resulted in reduction of the intracellular NAD^+ level. This attenuation of cellular NAD^+ was completely inhibited by ACPH. Such observations was also found for PARP inhibitors like ABT-888 in bis-[2-chloroethyl] sulfide (SM) treated HaCaT cells [50] and with the inhibitor, PJ34 in peroxynitrite exposed cells in mice model [51]. The suppression of NAD^+ depletion in DNA damaged cells treated with ACPH confirmed its PARP1 inhibitory action.

Selective localization of drugs in tissue is an important aspect in the study of pharmacokinetics of drugs. Considering the importance of ACPH as an anticancer agent from our earlier studies [17] Liu et al. have evaluated the retention of ACPH in the kidney of BAlb/c mice and the findings were promising [52]. The drug-like activity of a molecule is judged by Lipinski rule; it provides some guideline to determine the effectiveness of a molecule as an oral drug candidate [29]. The drug activity of ACPH was analyzed and compared with the known PARP1 inhibitors (Table 3). Particularly significant was the AlogP value; it was found to be the maximum for ACPH. This would reflect the fact that ACPH would be more lipophilic and would have a better chance of getting absorbed by body cells and might have a better chance of being retained in the body. The other parameters of ACPH were also similar to the other known PARP1 inhibitors.

CONCLUSION

In view of the role of PARP1 in different cellular processes, its inhibitors are important in the patho-physiology of different diseases. Particularly noteworthy is its role in cancer therapy. We have demonstrated for the first time the positive role of ACPH as a PARP1 inhibitor. Our findings are important as it indicates the potential of ACPH as a drug candidate. These finding may be vital for new drug development using acridine based molecule as PARP1 inhibitors.

ACKNOWLEDGEMENT

The authors acknowledge the Bioinformatics Facility at BIF centre, University of Kalyani for this work. Authors also acknowledge financial assistance from University of Kalyani, Kalyani and DST-PURSE, Govt. of India along with DST-FIST, Govt. of India for instrumental facilities in the department. S.K, S.H, D.M, S.G, and A.M are supported by UGC-BSR, UGC-RGNF, URS-Kalyani University and DST-INSPIRE fellowship respectively. Some of these results were presented in 9th Indo Global Summit on Cancer Therapy, the OMICS international conference.

Conflict of interest: There is no conflict of interest.

REFERENCES

[1] CR Caffrey; D Steverding; RK Swenerton; B Kelly; D Walshe; A Debnath; KM Land. *Antimicrob Agents Chemother*. **2007**, 51(6), 2164-2172.
[2] SA Lyakhov; YI Suveyzdis; LA Litvinova; SA Andronati; SL Rybalko; ST Dyadyun. *Pharmazie*. **2000**, 55(10), 733-736.
[3] M Wainwright. *J Antimicrob Chemother*. **2001**, 47(1), 1-13.
[4] M Demeunynck. *Expert Opin Ther Pat.* **2004**, 14(1), 55-70.
[5] E Kuruvilla; J Joseph; D Ramaiah. *J Phys Chem B.* **2005**, 109(46), 21997-22002.
[6] R Ghosh; S Bhowmik; A Bagchi; D Das; S Ghosh. *Eur Biophys J*. **2010**, 39(8), 1243-1249.
[7] J Kaur; P Singh. *Expert Opin Ther Pat.* **2011**, 21(4), 437-454.
[8] R Ferreira; R Artali; A Benoit; R Gargallo; R Eritja; DM Ferguson; S Mazzini. *PloS one*. **2013**, 8(3), e57701.
[9] E Verdaguer; EG Jordà; AM Canudas; A Jiménez; FX Sureda; V Rimbau; A Camins. *Neuroscience.* **2003**, 120(3), 599-603.
[10] S Bhowmik; A Bagchi; R Ghosh. *Int J Integr Biol.* **2008**, 2(1), 8-14.
[11] S Sparapani; SM Haider; F Doria; M Gunaratnam; S Neidle. *J Am Chem Soc.* **2010**, 132(35), 12263-12272.
[12] R Preet; P Mohapatra; S Mohanty; SK Sahu; T Choudhuri; MD Wyatt; CN Kundu. *Int J Cancer*. **2012**, 130(7), 1660-1670.
[13] S Karmakar; R Ghosh. *Int J Sci Res.* **2015**, 4(12), 1362-1366.
[14] R Krishnakumar; WL Kraus. *Mol Cell.* **2010**, 39(1), 8-24.
[15] A Peralta-Leal; JM Rodríguez-Vargas; R Aguilar-Quesada; MI Rodríguez; JL Linares; MR de Almodóvar; FJ Oliver. *Free Radic Biol Med.* **2009**, 47(1), 13-26.
[16] L Virág; C Szabó. *Pharmacol Rev.* **2002**, 54(3), 375-429.
[17] R Ghosh; S Bhowmik; D Guha. *Mol Cell Biochem.* **2012**, 361(1-2), 55-66.
[18] NI Ryabokon; RI Goncharova; G Duburs; J Rzeszowska-Wolny. *Mutat Res-Gen Tox En.* **2005**, 587(1), 52-58.
[19] V Schreiber; F Dantzer; JC Ame; G De Murcia. *Nat Rev Mol Cell Biol.* **2006**, 7(7), 517-528.
[20] AR Gangloff; J Brown; R De Jong; DR Dougan; CE Grimshaw; M Hixon; E Taylor. *Bioorg Med Chem Lett.* **2013**, 23(16), 4501-4505.

[21] MA Lill; ML Danielson. *J Comput Aided Mol Des.* **2011**, 25(1), 13-19.
[22] BR Brooks; RE Bruccoleri; BD Olafson; DJ States; S Swaminathan; M Karplus. *J Comput Chem.* **1983**, 4(2), 187-217.
[23] GM Morris; DS Goodsell; RS Halliday; R Huey; WE Hart; RK Belew; AJ Olson. *J Comput Chem.* **1998**, 19(14), 1639-1662.
[24] D Schneidman-Duhovny; Y Inbar; R Nussinov; HJ Wolfson. *Nucleic Acids Res.* **2005**, 33(S2), W363-W367.
[25] G Jones; P Willett; RC Glen; AR Leach; R Taylor. *J Mol Biol.* **1997**, 267(3), 727-748.
[26] B Hess; C Kutzner; D Van Der Spoel; E Lindahl. *J Chem Theory Comput.* **2008**, 4(3), 435-447.
[27] B Hess. *J Chem Theory Comput.* **2008**, 4(1), 116-122.
[28] U Essmann; L Perera; ML Berkowitz; T Darden; H Lee; LG Pedersen. *J Chem Phys.* **1995**, 103(19), 8577-8593.
[29] P Leeson. *Nature.* **2012**, 481(7382), 455-456.
[30] R Ghosh; D Guha; S Bhowmik; S Karmakar. *Mutat Res-Gen Tox En.* **2013**, 757(1), 83-90.
[31] M Kosloff; R Kolodny. *Proteins.* **2008**, 71(2), 891-902.
[32] W Swegat; J Schlitter; P Krüger; A Wollmer. *Biophys J.* **2003**, 84(3), 1493-1506.
[33] J Li; N Zhou; P Cai; J Bao. *Int J Mol Sci.* **2016**, 17(2), 258.
[34] K Ohno; T Mitsui; Y Tanida; A Matsuura; H Fujitani; T Niimi; M Orita. *J Mol Model*. **2011**, 17(2), 383-389.
[35] AM Gallina; P Bork; D Bordo. *J Mol Recogn.* **2014**, 27(2), 65-72.
[36] T Kinoshita; I Nakanishi; M Warizaya; A Iwashita; Y Kido; K Hattori; T Fujii. *FEBS Lett.* **2004**, 556(1-3), 43-46.
[37] G Costantino; A Macchiarulo; E Camaioni; R Pellicciari. *J Med Chem.* **2001**, 44(23), 3786-3794.
[38] A Ruf; JM De Murcia; G De Murcia; GE Schulz. *P Natl Acad Sci USA*. **1996**, 93(15), 7481-7485.
[39] Y Shen; M Aoyagi-Scharber; B Wang. *J Pharm Exp Ther.* **2015**, 353(3), 446-457.
[40] A Ruf; G De Murcia; GE Schulz. *Biochemistry*. **1998**, 37(11), 3893-3900.
[41] A Ruf; V Rolli; G de Murcia; GE Schulz. *J Mol Biol.* **1998**, 278(1), 57-65.
[42] J Miyashiro; KW Woods; CH Park; X Liu; Y Shi; EF Johnson; VL Giranda. *Bioorg Med Chem Lett.* **2009**, 19(15), 4050-4054.
[43] GT Marsischky; BA Wilson; RJ Collier. *J Biol Chem.* **1995**, 270(7), 3247-3254.
[44] NJ Curtin. PARP inhibitors and cancer therapy. In: A Bürkle, Poly(ADP-Ribosyl)ation, Landes Bioscience and Springer Science, Georgetown, TX, USA, **2006**, 218-233.
[45] H Farmer; N McCabe; CJ Lord; AN Tutt; DA Johnson; TB Richardson; A Ashworth. *Nature*. **2005**, 434(7035), 917-921.
[46] DA Boothman; HL Burrows; CR Yang; TD Davis; SM Wuerzberger; SM Planchon; TJ Kinsella. *Stem Cells*. **1997**, 15(S1), 27-42.
[47] HR Mellor; DJP Ferguson; R Callaghan. *British J Cancer*, **2005**, 93(3), 302-309.
[48] S Boulton; LC Pemberton; JK Porteous; NJ Curtin; RJ Griffin; BT Golding; BW Durkacz. *British J Cancer*. **1995**, 72(4), 849-856.
[49] JA De Soto; R Mullins. *J Clin Oncol.* **2011**, 29, e13542.
[50] F Liu; N Jiang; ZY Xiao; JP Cheng; YZ Mei; P Zheng; YX Zhang. *Peer J*. **2016**, 4, e1890.
[51] CC Alano; P Garnier; W Ying; Y Higashi; TM Kauppinen; RA Swanson. *J Neurosci.* **2010**, 30(8), 2967-2978.
[52] P Liu; Y Hu; J Chen; Q Yang. *Rapid Commun. Mass Spectrom*. **2015**, 29(14), 1328-1334.